Chemical Engineering Communications
Publication details, including instructions for authors and subscription information:
http://www.informaworld.com/smpp/title~content=t713454788

UNSTEADY MIXED CONVECTION WITH SORET AND DUFOUR EFFECTS PAST A POROUS PLATE MOVING THROUGH A BINARY MIXTURE OF CHEMICALLY REACTING FLUID

O. D. Makinde[a]; P. O. Olanrewaju[b]
[a] Faculty of Engineering, Cape Peninsula University of Technology, Bellville, South Africa [b] Department of Mathematics, Covenant University, Canaanland, Ota, Nigeria

Online publication date: 09 March 2011

To cite this Article Makinde, O. D. and Olanrewaju, P. O.(2011) 'UNSTEADY MIXED CONVECTION WITH SORET AND DUFOUR EFFECTS PAST A POROUS PLATE MOVING THROUGH A BINARY MIXTURE OF CHEMICALLY REACTING FLUID', Chemical Engineering Communications, 198: 7, 920 — 938
To link to this Article: DOI: 10.1080/00986445.2011.545296
URL: http://dx.doi.org/10.1080/00986445.2011.545296

Chem. Eng. Comm., 198:920–938, 2011

ISSN: 0098-6445 print/1563-5201 online
DOI: 10.1080/00986445.2011.545296

Taylor & Francis
Taylor & Francis Group

Unsteady Mixed Convection with Soret and Dufour Effects Past a Porous Plate Moving through a Binary Mixture of Chemically Reacting Fluid

O. D. MAKINDE[1] AND P. O. OLANREWAJU[2]

[1]Faculty of Engineering, Cape Peninsula University of Technology, Bellville, South Africa
[2]Department of Mathematics, Covenant University, Canaanland, Ota, Nigeria

This study investigates the unsteady mixed convection flow past a vertical porous flat plate moving through a binary mixture in the presence of radiative heat transfer and nth-order Arrhenius type of irreversible chemical reaction by taking into account the diffusion-thermal (Dufour) and thermo-diffusion (Soret) effects. Assuming an optically thin radiating fluid and using a local similarity variable, the governing nonlinear partial differential equations have been transformed into a set of coupled nonlinear ordinary differential equations, which are solved numerically by applying shooting iteration technique together with fourth-order Runge-Kutta integration scheme. Graphical results for the dimensionless velocity, temperature, and concentration distributions are shown for various values of the thermophysical parameters controlling the flow regime. Finally, numerical values of physical quantities, such as the local skin-friction coefficient, the local Nusselt number, and the local Sherwood number are presented in tabular form.

Keywords Arrhenius kinetics; Binary mixture; Boundary layer flow; Porous plate; Radiative heat; Soret and Dufour effects

Introduction

Mixed convection boundary layer flow of a binary mixture of fluids with heat and mass transfer past a continuous moving surface has attracted considerable attention in the past several decades, due to its many important engineering and industrial applications (Jaluria, 1980; Schlichting, 1979). In nature such flows are encountered in the oceans, lakes, solar ponds, and the atmosphere. They are also responsible for the geophysics of planets. In industry, a familiar example of a binary mixture of fluids is an emulsion, which is the dispersion of one fluid within another fluid. Typical emulsions are oil dispersed within water or water within oil. Another example where the mixture of fluids plays an important role is in multigrade oils. Polymeric-type fluids are added to the base oil so as to enhance the lubrication properties of mineral oil. Moreover, the mixed convection boundary layer problem

Address correspondence to O. D. Makinde, Institute for Advanced Research in Mathematical Modelling and Computations, Cape Peninsula University of Technology, P. O. Box 1906, Bellville 7535, South Africa. E-mail: makinded@cput.ac.za

is also encountered in aerodynamic extrusion of plastic and rubber sheets, cooling of an infinite metallic plate in a cooling path, which may be an electrolyte, crystal growing, the boundary layer along a liquid film in condensation processes, and a polymer sheet or filament extruded continuously from a die or along thread traveling between a feed roll and a windup roll are examples of practical applications of continuous moving surfaces.

Several studies on boundary layer flow coupled with heat and mass transfer have already appeared in the literature (Chandrasekhara et al., 1992; Chamkha and Khaled, 2000; Makinde, 2005; Makinde and Ogulu, 2008; Ogulu and Makinde, 2009). In all these studies Soret-Dufour effects were assumed to be negligible. In combined heat and mass transfer processes, the thermal energy flux resulting from concentration gradients is referred to as the Dufour or diffusion-thermal effect. Similarly, the Soret or thermo-diffusion effect is the contribution to the mass fluxes due to temperature gradients. Moreover, when chemical species are introduced at a surface in the fluid domain with different (lower) density than the surrounding fluid, both Soret (thermo-diffusion) and Dufour (diffusion-thermal) effects can be influential. The effect of diffusion-thermal and thermal diffusion of heat and mass has been developed from the kinetic theory of gases by Chapman and Cowling (1952) and Hirshfelder et al. (1954). They explained the phenomena and derived the necessary formulas to calculate the thermal diffusion coefficient and the thermal-diffusion factor for monatomic gases or for polyatomic gas mixtures. Kafoussias and Williams (1995) studied the thermal diffusion and the diffusion-thermal effects on mixed free-forced convective and mass transfer steady laminar boundary layer flow, over a vertical flat plate, with temperature dependent viscosity. Alam and Rahman (2006) studied the Dufour and Soret effects on mixed convection flow past a vertical porous flat plate with variable suction. Anghel et al. (2000) investigated the Dufour and Soret effects on free convection boundary layer over a vertical surface embedded in a porous medium. Postelnicu (2007) studied the influence of a magnetic field on heat and mass transfer by natural convection from a vertical surface embedded in an electrically conducting fluid-saturated porous medium considering Soret and Dufour effects with constant surface temperature and concentration. Alam et al. (2007) presented an analysis of the Soret and Dufour effects on free convective heat and mass transfer flow in a porous medium with time-dependent temperature and concentration. Bég et al. (2009) investigated numerically the free convection magnetohydrodynamic heat and mass transfer from a stretching surface to a saturated porous medium with Soret and Dufour effects. Various other aspects dealing with the Soret and Dufour effects on steady boundary layer flow with combined heat and mass transfer problems have been reported (Afify, 2009; Chamkha and Ben-Nakhi, 2008; Tsai and Huang, 2009; Seddeek, 2004; Abdallah, 2009; Alam et al., 2006; Ferdows et al., 2008; El-Aziz, 2008).

In spite of all these investigations reported in the literature, the thermo-diffusion and diffusion-thermal effects on unsteady mixed convection with heat and mass transfer have not yet been studied. Hence, based on the above-mentioned investigations and applications, the present article considers unsteady mixed convection with Dufour and Soret effects past a vertical porous plate moving through a binary mixture in the presence of radiative heat transfer and nth-order Arrhenius-type chemical reaction. Numerical calculations were carried out for different values of the various dimensionless parameters controlling the flow regime. It is hoped that the results

obtained will not only provide useful information for applications, but also serve as a complement to the previous studies.

Mathematical Analysis

Consider unsteady one dimensional convective flow of an optically thin radiating incompressible fluid past a flat plate moving through a binary mixture (see Figure 1). Following Alam and Rahman (2006), we assume the Dufour effect may be described by a second-order concentration derivative with respect to the transverse coordinate in the energy conservation equation and the Soret effect by a second-order temperature derivative in the concentration equation.

Under these assumptions, along with Boussinesq's approximation, the governing equations for continuity, momentum, energy, and species diffusion in laminar incompressible boundary layer flow can be written as follows:

$$\frac{\partial v}{\partial y} = 0, \tag{1}$$

$$\frac{\partial u}{\partial t} + v\frac{\partial u}{\partial y} = \upsilon\frac{\partial^2 u}{\partial y^2} + g\beta(T - T_\infty) + g\beta_c(C - C_\infty) \tag{2}$$

$$\rho c_p\left(\frac{\partial T}{\partial t} + v\frac{\partial T}{\partial y}\right) = k\frac{\partial^2 T}{\partial y^2} + Q - 4\sigma\alpha T^4 + \frac{\rho D k_T}{c_s}\frac{\partial^2 C}{\partial y^2} \tag{3}$$

$$\frac{\partial C}{\partial t} + v\frac{\partial C}{\partial y} = D\frac{\partial^2 C}{\partial y^2} - R_A + \frac{Dk_T}{T_m}\frac{\partial^2 T}{\partial y^2} \tag{4}$$

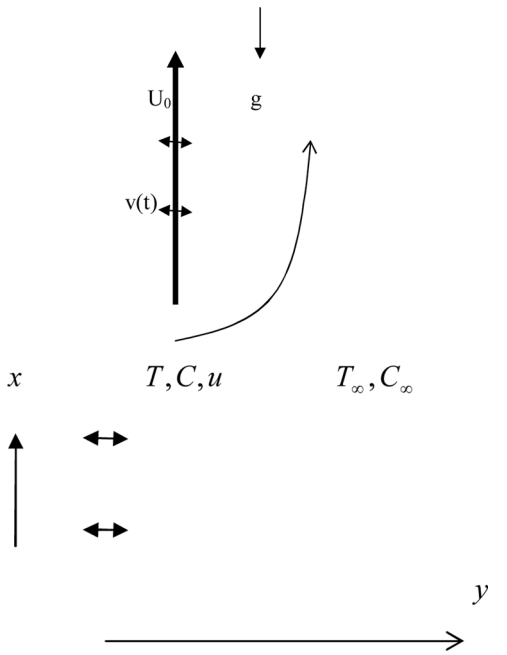

Figure 1. Flow configuration and coordinate system.

where u and v are velocity components in x and y directions respectively, T is the temperature, t is the time, g is the acceleration due to gravity, α is the absorption coefficient, k_T is the thermal diffusion ratio, c_s is the concentration susceptibility, T_m is the mean fluid temperature, σ is the Stefan-Boltzmann constant, β is the thermal expansion coefficient, β_c is the concentration expansion coefficient, υ is the kinematic viscosity, D is the chemical molecular diffusivity, k is the thermal conductivity, ρ is the density, T_w is the wall temperature, T_∞ is the free stream temperature, C_w is the species concentration at the plate surface, C_∞ is the free stream concentration, $Q=(-\Delta H)R_A$ is the heat of chemical reaction, and ΔH is the activation enthalpy. For an optically thin fluid $\alpha \ll 1$, and the approximate form of the flux equation (Cheng, 1964) is utilized in Equation (3). We employed Arrhenius type of the nth-order irreversible reaction given by (Kamenetskii, 1969)

$$R_A = k_r e^{-E/R_G T} C^n \tag{5}$$

where k_r is the chemical reaction rate, R_G is the universal gas constant, and E is the activation energy parameter. The appropriate initial and boundary conditions are

$$u(y,0) = 0, \quad T(y,0) = T_w, \quad C(y,0) = C_w \tag{6}$$

$$u(0,t) = U_0, \quad T(0,t) = T_w, \quad C(0,t) = C_w, \quad t > 0 \tag{7}$$

$$u \to 0, \quad T \to T_\infty, \quad C \to C_\infty \quad \text{as } y \to \infty, t > 0 \tag{8}$$

where U_0 is the plate characteristic velocity. We introduce the following dimensionless quantities and parameters:

$$u = U_0 F(\eta), \quad (\theta, \theta_w) = \frac{(T, T_w)}{T_\infty}, \quad (\varphi, \varphi_w) = \frac{(C, C_w)}{C_\infty}, \quad G_r = \frac{4\upsilon tg\beta T_\infty}{U_0},$$
$$Du = \frac{Dk_T C_\infty}{c_s T_\infty \rho c_p \upsilon}, \quad G_c = \frac{4\upsilon tg\beta_c C_\infty}{U_0}, \quad P_r = \frac{\upsilon}{\lambda}, \quad \lambda = \frac{k}{\rho c_p}, \quad S_c = \frac{\upsilon}{D},$$
$$\gamma = \frac{E}{R_G T_\infty}, \quad \eta = \frac{y}{2\sqrt{\upsilon t}}, \quad Sr = \frac{Dk_T T_\infty}{\rho T_m C_\infty}, \quad k_0 = k_r e^{-\frac{E}{R_G T_\infty}}, \quad b = \frac{(-\Delta H)C_\infty}{\rho c_p T_\infty},$$
$$Ra = \frac{16\sigma\alpha t T_\infty^3}{\rho c_p}, \quad Da = 4tk_0 C_\infty^{n-1}. \tag{9}$$

From Equation (1), v is either constant or a function of time. Following Makinde (2005), we choose

$$v = -c\left(\frac{\upsilon}{t}\right)^{\frac{1}{2}}, \tag{10}$$

where c > 0 is the suction parameter and c < 0 is the injection parameter. Equations (2)–(4) then become

$$F'' + 2(\eta + c)F' = -G_r(\theta - 1) - G_c(\varphi - 1) \tag{11}$$

$$\frac{1}{p_r}\theta'' + 2(\eta + c)\,\theta' + Du\varphi'' = -bDa\varphi^n \exp\left(\gamma\left(1-\frac{1}{\theta}\right)\right) + Ra\theta^4 \tag{12}$$

$$\frac{1}{Sc}\varphi'' + 2(\eta + c)\,\varphi' + Sr\theta'' = Da\varphi^n \exp\left(\gamma\left(1-\frac{1}{\theta}\right)\right) \tag{13}$$

with the boundary conditions

$$\begin{aligned} &F(0) = 1,\ \theta(0) = \theta_w,\ \varphi(0) = \varphi_w, \\ &F(\infty) = 0,\ \theta(\infty) = 1,\ \varphi(\infty) = 1, \end{aligned} \tag{14}$$

where the prime symbol denotes differentiation with respect to η, b is the heat generation parameter, Da is the Damköhler number, Ra is the radiation parameter, γ is the activation energy parameter, G_r is the local thermal Grashof number, G_c is the local solutal Grashof number, Sr is the Soret number, and Du is the Dufour number. Also, other quantities of physical interest in this problem are the local skin friction (C_f), local Nusselt number (Nu), and Sherwood numbers (Sh), which are defined by

$$C_f = \frac{2\upsilon\sqrt{t}}{U_0\sqrt{\upsilon}}\frac{\partial u}{\partial y}\bigg|_{y=0} = F'(0) \tag{15}$$

$$Nu = -\frac{2\sqrt{\upsilon t}}{T_\infty}\frac{\partial T}{\partial y}\bigg|_{y=0} = -\theta'(0) \tag{16}$$

$$Sh = -\frac{2\sqrt{\upsilon t}}{C_\infty}\frac{\partial C}{\partial y}\bigg|_{y=0} = -\varphi'(0) \tag{17}$$

and from that we can easily compute the results of the local skin friction, local Nusselt number, and local Sherwood number.

Numerical Procedure

The coupled nonlinear differential equations (11)–(13) with the boundary conditions in (14) are solved computationally using the fourth-order Runge-Kutta method with a shooting technique and implemented on Maple software (Maplesoft, Waterloo, Ont., Canada). The details of the solution method are omitted here to conserve space. The step size 0.001 is used to obtain the numerical solution with seven-decimal place accuracy as the criterion of convergence.

Results and Discussion

For the present problem numerical computations are carried out by employing the similarity solution for all η and different values of the thermophysical parameters controlling the fluid dynamics in the flow regime. The values of the Schmidt number (Sc) are chosen for hydrogen ($Sc = 0.22$), water vapor ($Sc = 0.62$), and ammonia ($Sc = 0.78$) at 25°C and one atmospheric pressure. The value of the Prandtl number is chosen to be $Pr = 0.71$, which represents air at 25°C and one atmospheric pressure.

Table I. Comparison of the values of C_f, Nu, and Sh for $G_r = G_c = 5$, $Ra = 0.1$, $n = Da = Du = Sr = 0$, $\theta_w = \varphi_w = 1$

C	Sc	Pr	C_f Makinde, 2005	Nu Makinde, 2005	Sh Makinde, 2005	C_f present	Nu present	Sh Present
0.15	0.5	0.71	3.30826	1.11600	0.89576	3.31492	0.98386	0.89576
0.25	0.5	0.71	3.09046	1.21262	0.96355	3.09685	1.06916	0.96355
0.25	0.7	0.71	2.77995	1.21262	1.17758	2.78579	1.06916	1.17758
0.25	1.0	0.71	2.47789	1.21262	1.46476	2.48389	1.06916	1.46476
0.25	0.5	0.90	2.88371	1.40022	0.96355	2.88953	1.23461	0.96355
0.25	0.5	1.00	2.79575	1.49399	0.96355	2.80154	1.31725	0.96355

Attention is focused on positive values of the buoyancy parameters, i.e., local thermal Grashof number $G_r > 0$ (which corresponds to the cooling problem) and local solutal Grashof number $G_c > 0$ (which indicates that the chemical species concentration in the free stream region is less than the concentration at the boundary surface). The cooling problem is often encountered in engineering applications, for example, in the cooling of electronic components and nuclear reactors. It should be mentioned here that $Da > 0$ indicates an increase in the destructive chemical reaction rate, while $Da < 0$ corresponds to an increase in generative chemical reaction rate. In order to check our computational method for numerical accuracy, we compare a special case of this present study ($n = Da = Du = Sr = 0$) with the numerical data from a previously published paper (Makinde, 2005); as shown in Table I, the results obtained are in perfect agreement. From Table II, it is seen that the local skin friction on the plate surface increases with increasing parameter values of Ra, n, G_r, G_c, Sr, Du, Sc, $c > 0$ and decreases with increasing values of Sc, Da. The local heat transfer rate at the plate surface (Nu) increases with increasing values of Da, Sr, $c > 0$ and decreases with increasing values of Sc, Ra, n, Du. Further, it is found that the local Sherwood number at the plate surface increases with an increase in Sc, Ra, n, Du, $c > 0$ and decreases with increasing values of Da, Sr.

Velocity Profiles

Figures 2 and 3 depict the effect of buoyancy forces (G_r and G_c) on the fluid velocity within the boundary layer. The fluid velocity is highest at the moving plate surface, decreases gradually with the occurrence of reverse flow within the boundary layer, and eventually straightens out to the free stream zero value far away from the plate, satisfying the boundary condition. However, the momentum boundary layer thickness generally decreases as the parameter values of G_r and G_c increase in the presence of uniform suction at the plate surface. It is interesting to note that the down peak of reverse flow velocity within the boundary layer increases as the intensity of buoyancy forces increases, i.e., with gradual increase in the parameter values of G_r and G_c. Figure 4 represents the velocity profiles for different values of suction/injection parameter. It is observed that the momentum boundary layer thickness decreases with suction ($c > 0$) and increases with injection ($c < 0$). This is in agreement with the usual fact that suction stabilizes the boundary layer growth, as reported by Alam

Table 2. Computations showing values of $\varphi'(0)$, $F'(0)$, and $\theta'(0)$ for $b=1$, $Pr=0.71$, $\gamma=\theta_w=\varphi_w=1$

Da	Sc	c	Ra	n	G_r	G_c	Sr	Du	$F'(0)$	$-\varphi'(0)$	$-\theta'(0)$
0.1	0.22	0.1	0.1	1	0.1	0.1	0.1	0.1	1.3643409	0.43942224	0.92901581
0.2	0.22	0.1	0.1	1	0.1	0.1	0.1	0.1	1.3636363	0.39356836	1.00765281
0.3	0.22	0.1	0.1	1	0.1	0.1	0.1	0.1	1.3631537	0.35169895	1.07685504
0.1	0.62	0.1	0.1	1	0.1	0.1	0.1	0.1	1.3493964	0.73498767	0.92488023
0.1	0.78	0.1	0.1	1	0.1	0.1	0.1	0.1	1.3465930	0.82617175	0.92177805
0.1	0.22	1.0	0.1	1	0.1	0.1	0.1	0.1	2.7395646	0.65675647	1.76910475
0.1	0.22	−0.1	0.1	1	0.1	0.1	0.1	0.1	1.1089790	0.39608977	0.77089113
0.1	0.22	−1.0	0.1	1	0.1	0.1	0.1	0.1	0.3113181	0.22742720	0.24525865
0.1	0.22	0.1	0.2	1	0.1	0.1	0.1	0.1	1.3712201	0.44081956	0.85696810
0.1	0.22	0.1	0.3	1	0.1	0.1	0.1	0.1	1.3767368	0.44190333	0.80218646
0.1	0.22	0.1	0.1	3	0.1	0.1	0.1	0.1	1.3646601	0.45173257	0.90246855
0.1	0.22	0.1	0.1	5	0.1	0.1	0.1	0.1	1.3647969	0.45706060	0.89220730
0.1	0.22	0.1	0.1	1	1.0	0.1	0.1	0.1	1.7225061	0.43942224	0.92901581
0.1	0.22	0.1	0.1	1	5.0	0.1	0.1	0.1	3.3143516	0.43942224	0.92901581
0.1	0.22	0.1	0.1	1	0.1	1.0	0.1	0.1	1.9568561	0.43942224	0.92901581
0.1	0.22	0.1	0.1	1	0.1	5.0	0.1	0.1	4.5902569	0.43942224	0.92901581
0.1	0.22	0.1	0.1	1	0.1	0.1	0.5	0.1	1.3667731	0.38493735	0.93009986
0.1	0.22	0.1	0.1	1	0.1	0.1	1.0	0.1	1.3698136	0.31655252	0.93147352
0.1	0.22	0.1	0.1	1	0.1	0.1	0.1	0.5	1.3663249	0.44026995	0.88601896
0.1	0.22	0.1	0.1	1	0.1	0.1	0.1	1.0	1.3688255	0.44135115	0.83143833

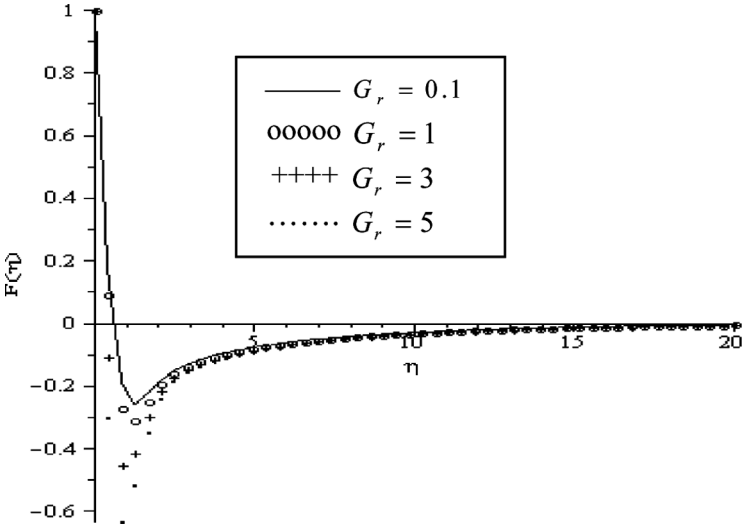

Figure 2. Effects of thermal Grashof number on the velocity profiles when $G_c=2$, $\gamma=Ra=Da=\theta_w=\varphi_w=\mathrm{c}=0.1$, $Du=0.3$, $Sr=0.5$, $b=1$, $n=2$, $Sc=0.62$.

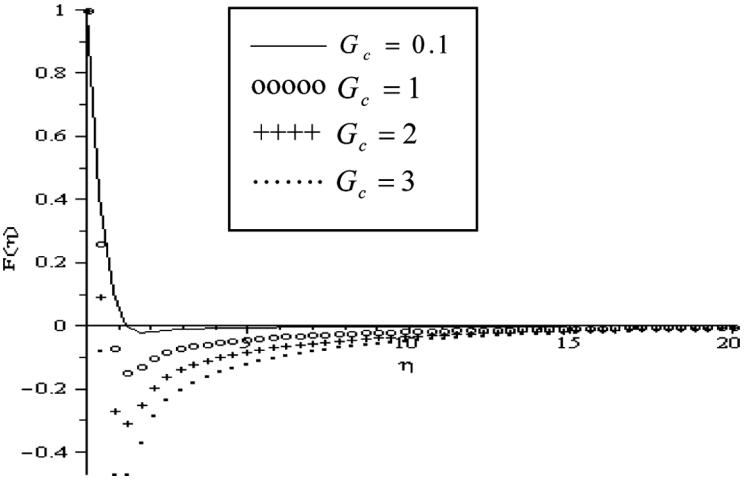

Figure 3. Effects of solutal Grashof number on the velocity profiles when $G_r = 1$, $\gamma = Ra = Da = \theta_w = \varphi_w = \mathrm{c} = 0.1$, $b = 1$, $n = 2$, $Du = 0.3$, $\mathrm{Sr} = 0.5$, $Sc = 0.62$.

and Rahman (2006). Moreover, a similar trend of flow reversal within the boundary layer also occurs and the lowest peak of the reverse flow velocity is enhanced by injection. Figure 5 represents the velocity profiles for different values of Soret and Dufour numbers and constant values of other physical parameters. It is observed that the velocity of fluid decreases with an increase of Soret number and a decrease of Dufour number. The lowest peak of the reverse flow velocity corresponds to the highest Soret number and lowest Dufour number. Figure 6 shows the effect of thermal radiation over the velocity profiles. It is observed that the velocity of the fluid

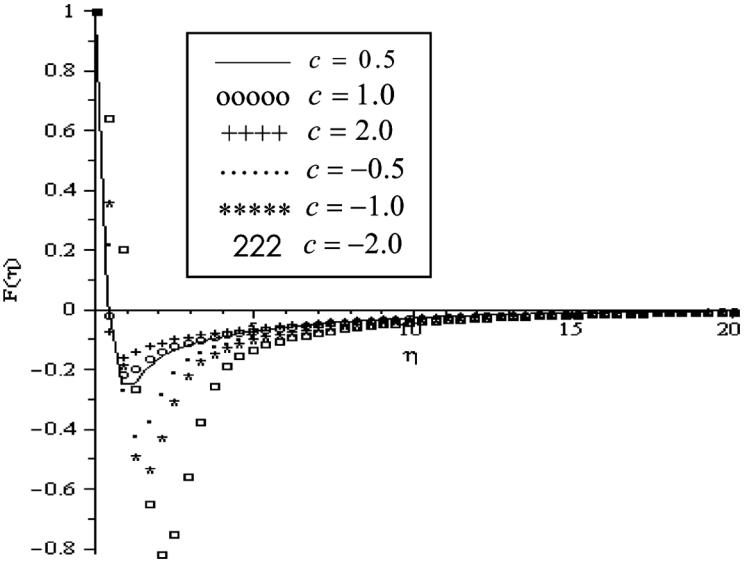

Figure 4. Effects of suction/injection parameter on the velocity profiles when $G_c = 2$, $G_r = 1$, $\gamma = Ra = Da = \theta_w = \varphi_w = 0.1$, $b = 1$, $n = 2$, $Du = 0.3$, $Sr = 0.5$, $Sc = 0.62$.

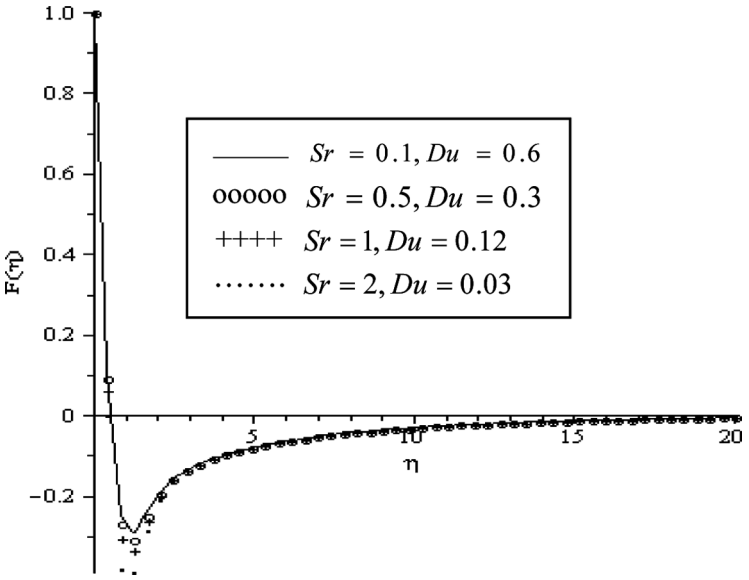

Figure 5. Soret with Dufour effect over the velocity profiles when $G_c = 2$, $G_r = 1$, $\gamma = Ra = Da = \theta_w = \varphi_w = 0.1$, $b = 1$, $n = 2$, $Sc = 0.62$.

decreases with an increase in the parameter values of Ra. It is worth mentioning that an increase in thermal radiation parameter (Ra) indicates an increase in radiative heat loss to the ambient, thereby augmenting the fluid cooling rate and flow reversal within the boundary layer. From Figure 7, it is observed that the velocity of the fluid

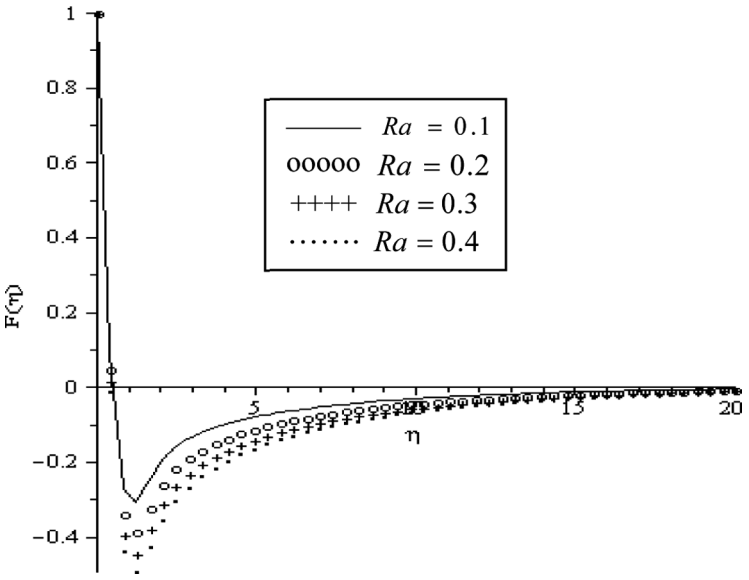

Figure 6. Effects of thermal radiation on the velocity profiles when $Du = 0.3$, $Sr = 0.5$, $G_r = 1$, $G_c = 2$, $Da = \gamma = \theta_w = \varphi_w = c = 0.1$, $b = 1$, $n = 2$, $Sc = 0.62$.

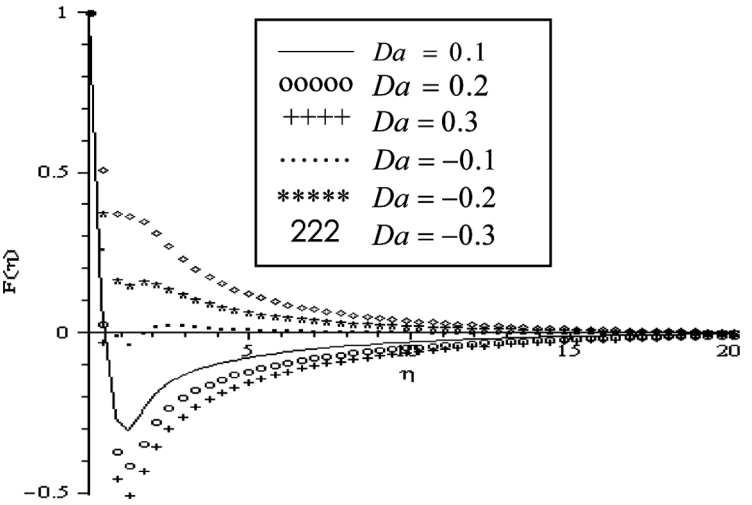

Figure 7. Effects of Damköhler number on the velocity profiles when $Du = 0.3$, $Sr = 0.5$, $G_r = 1$, $G_c = 2$, $\gamma = Ra = \theta_w = \varphi_w = \mathrm{c} = 0.1$, $b = 1$, $n = 2$, $Sc = 0.62$.

increases with an increase in generative chemical kinetics ($Da < 0$) and decreases with an increase in destructive chemical reaction rate ($Da > 0$). It is noteworthy that the flow reversal within the boundary layer is enhanced by an increase in the rate of destructive chemical reaction.

Temperature Profiles

The effects of various thermophysical parameters on the fluid temperature are illustrated in Figures 8–13. Generally, the fluid temperature increases from the plate

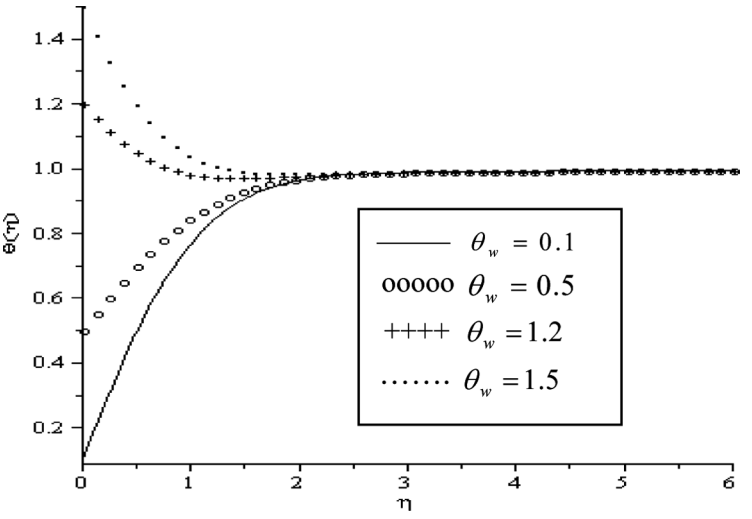

Figure 8. Effects of wall temperature variation on fluid temperature profiles when $Du = 0.3$, $Sr = 0.5$, $G_r = 1$, $\mathrm{G_c} = 2$, $\mathrm{Ra} = \gamma = Da = \varphi_w = \mathrm{c} = 0.1$, $b = 1$, $\mathrm{n} = 2$, $Sc = 0.62$.

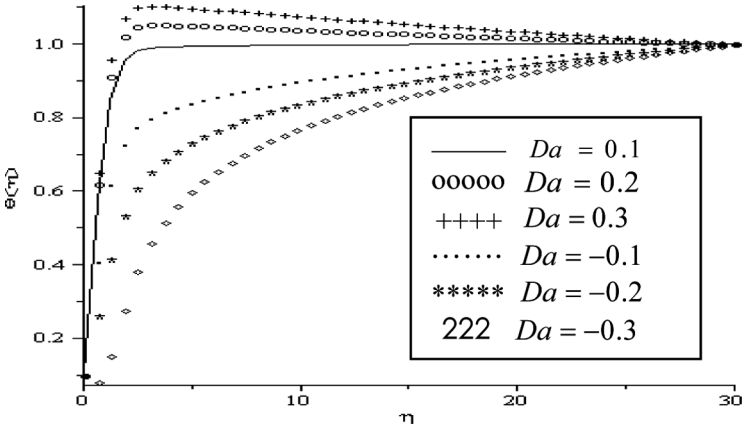

Figure 9. Effects of Damköhler number on the temperature profiles when $Du = 0.3$, $Sr = 0.5$, $G_r = 1$, $G_c = 2$, $\gamma = Ra = \theta_w = \varphi_w = c = 0.1$, $b = 1$, $n = 2$, $Sc = 0.62$.

surface and attains its peak value at the free stream whenever the plate surface temperature θ_w is lower than the free stream temperature. The trend is reversed whenever the plate surface temperature is higher than that of the free stream (see Figure 8). It is noteworthy that all the temperature profiles satisfy the far field boundary conditions asymptotically. Figure 9 shows that the temperature profiles increase with increasing Damköhler number ($Da > 0$) for destructive chemical reaction and decreases with increase in the generative chemical reaction rate ($Da < 0$). The increase in temperature when $Da > 0$ can be attributed to internal heat generation in the fluid due to Arrhenius kinetics. From Figure 10, it is observed that increase in the radiation parameter Ra decreases the temperature distribution in the thermal boundary layer. This is because large values of radiation parameter correspond to an increase in dominance of conduction over radiation, thereby decreasing the thickness of the thermal

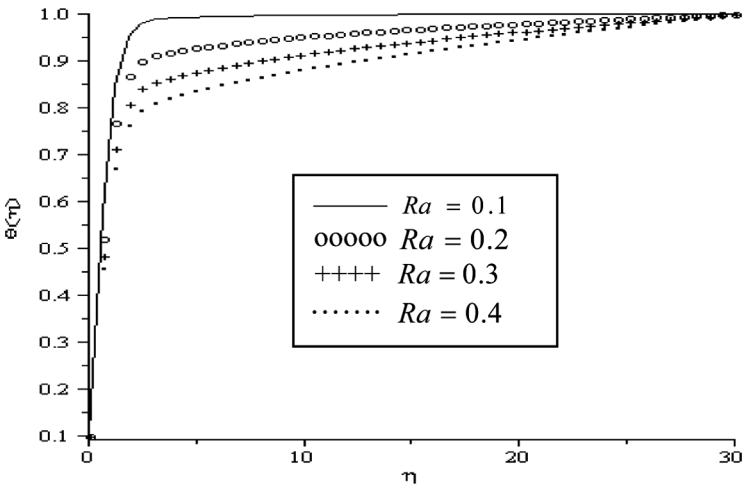

Figure 10. Effects of thermal radiation on the fluid temperature profiles when $Du = 0.3$, $Sr = 0.5$, $G_r = 1$, $G_c = 2$, $\gamma = Da = \theta_w = \varphi_w = c = 0.1$, $b = n = 1$, $Sc = 0.62$.

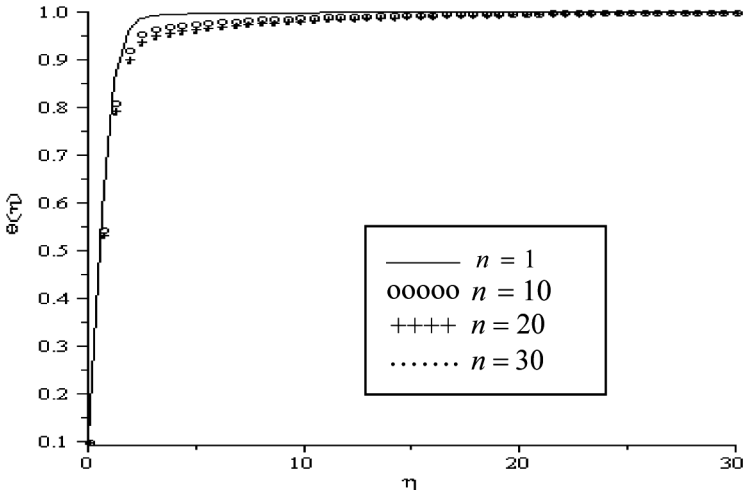

Figure 11. Effects of increasing reaction order on temperature profiles when $Du = 0.3$, $Sr = 0.5$, $G_r = 1$, $G_c = 2$, $Ra = \gamma = Da = \theta_w = \varphi_w = c = 0.1$, $b = 1$, $Sc = 0.62$.

boundary layer and increasing the heat loss to the ambient. Figure 11 depicts the variation of temperature profile against spanwise coordinate η for various values of reaction order index (n) and for fixed values of other physical parameters. It is observed from this figure that increase in reaction order index decreases temperature distribution throughout the boundary layer due to decrease in boundary layer thickness. Figure 12 depicts the variation of temperature profiles against η for different values of Soret and Dufour numbers and by fixing other physical parameters. From this graph we observe that fluid temperature profile increases slightly with an increase in Soret number (Sr) and a decrease in Dufour number (Du). This confirmed the recent observation by Tsai and Huang (2009). The effect of suction/injection

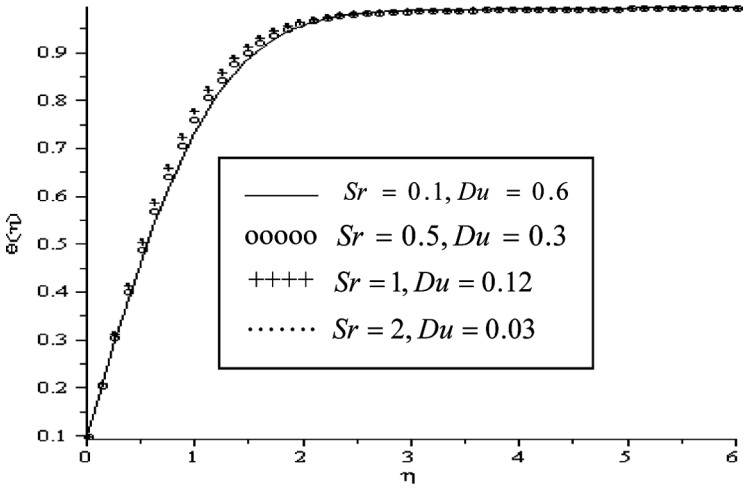

Figure 12. Soret with Dufour effect over the temperature profiles when $G_c = 2$, $G_r = 1$, $\gamma = Ra = Da = \theta_w = \varphi_w = 0.1$, $b = 1$, $n = 2$, $Sc = 0.62$.

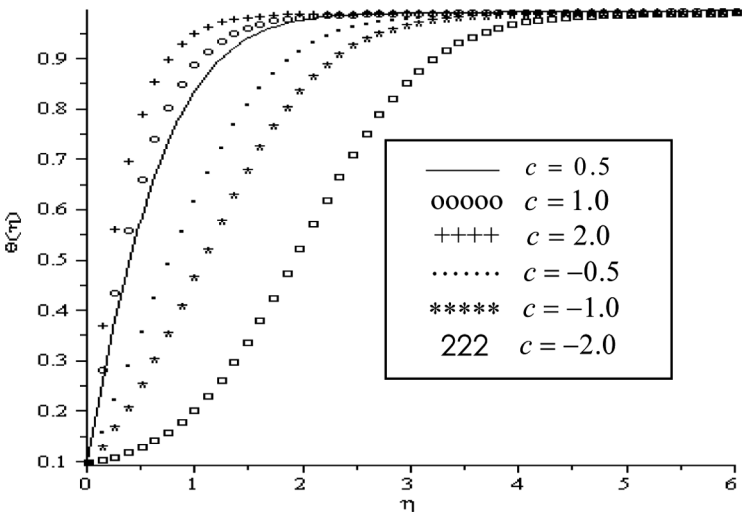

Figure 13. Effects of suction/injection on the temperature profiles with increasing values when $G_c = 2$, $G_r = 1$, $\gamma = Ra = Da = \theta_w = \varphi_w = 0.1$, $b = 1$, $n = 2$, $Du = 0.3$, $Sr = 0.5$, $Sc = 0.62$.

parameter on the fluid temperature is highlighted in Figure 13. It is observed that the fluid temperature increases with suction and decreases with injection.

Concentration Profiles

Figures 14–19 depict chemical species concentration profiles against spanwise coordinate η for varying values of physical parameters in the boundary layer. It is noteworthy that the species concentration increases from the plate surface and attains its

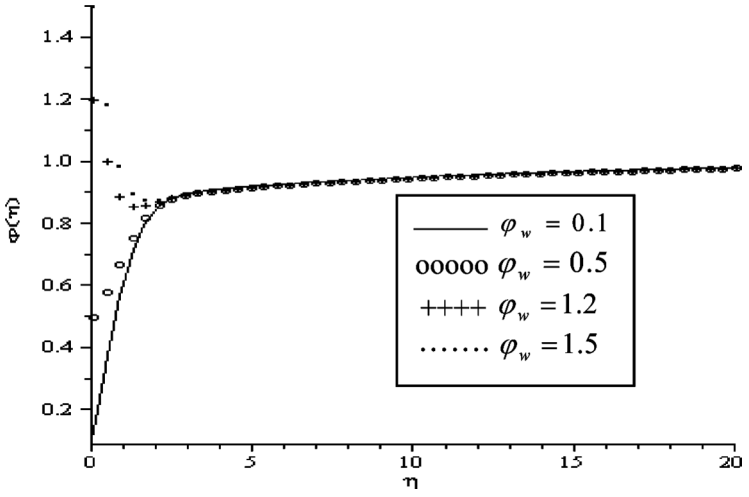

Figure 14. Variation of the boundary layer concentration profiles with increasing species concentration at the plate when $G_r = 1$, $G_c = 2$, $Ra = \gamma = Da = \theta_w = c = 0.1$, $b = 1$, $n = 2$, $Du = 0.3$, $Sr = 0.5$, $Sc = 0.62$.

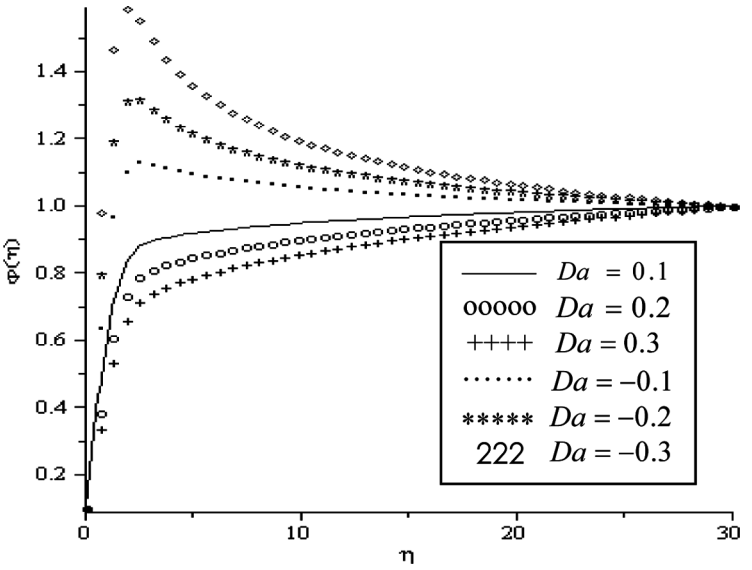

Figure 15. Effects of Damköhler number on the concentration profiles when $Du = 0.3$, $Sr = 0.5$, $G_r = 1$, $G_c = 2$, $\gamma = Ra = \theta_w = \varphi_w = \mathrm{c} = 0.1$, $b = 1$, $n = 2$, $Sc = 0.62$.

peak value at free stream whenever the concentration at the plate surface φ_w is lower than that of the free stream. The trend is reversed whenever the species concentration at the plate surface is higher than that of the free stream (see Figure 14). We remark here that all the concentration profiles satisfy the far field boundary conditions asymptotically. The effect of chemical reaction rate parameter (Da) on the species concentration profiles is shown in Figure 15. From the graph we observe that there

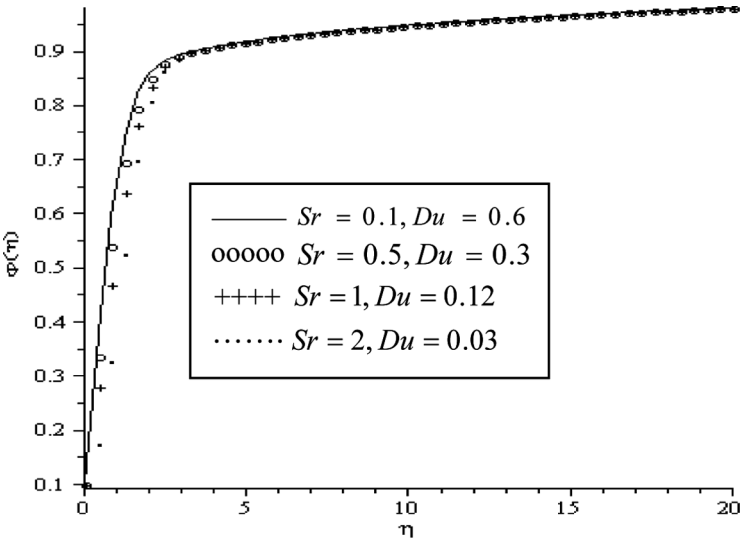

Figure 16. Soret with Dufour effect over the concentration profiles when $G_c = 2$, $G_r = 1$, $\gamma = Ra = Da = \theta_w = \varphi_w = 0.1$, $b = 1$, $n = 2$, $Sc = 0.62$.

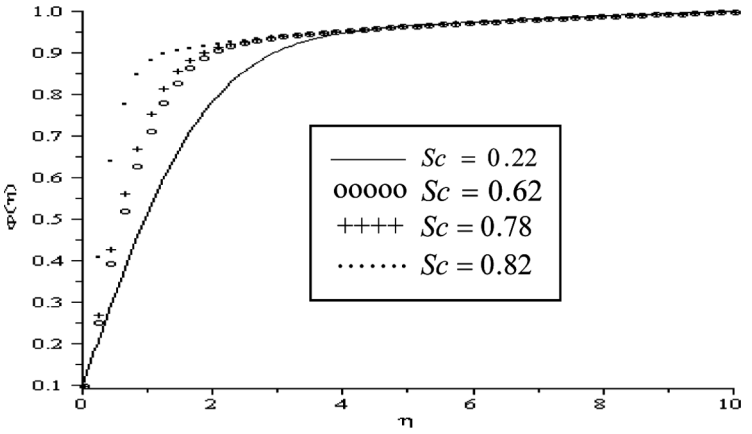

Figure 17. Effects of Schmidt number on the concentration profiles when $Du = 0.3$, $Sr = 0.5$, $G_r = 1$, $G_c = 2$, $Ra = \gamma = Da = \theta_w = \varphi_w = c = 0.1$, $b = 1$, $n = 2$.

is a marked effect of increasing value of both destructive and generative chemical reaction on concentration distribution in the boundary layer. Further, it is observed that increasing the value of the destructive chemical reaction rate ($Da > 0$) decreases the concentration of species within the boundary layer; this is due to the fact that destructive chemical reaction reduces the solutal boundary layer thickness and increases the mass transfer. The trend is reversed for generative chemical reaction ($Da < 0$); the species concentration increases, attains its peak value within the boundary layer, and decreases to the free stream value far away from the plate. Moreover, the peak value of the species concentration profile increases with an increase in generative chemical reaction rate. Figure 16 is a plot of concentration profiles against η for various values of Soret and Dufour numbers. As seen from the graph, an increase

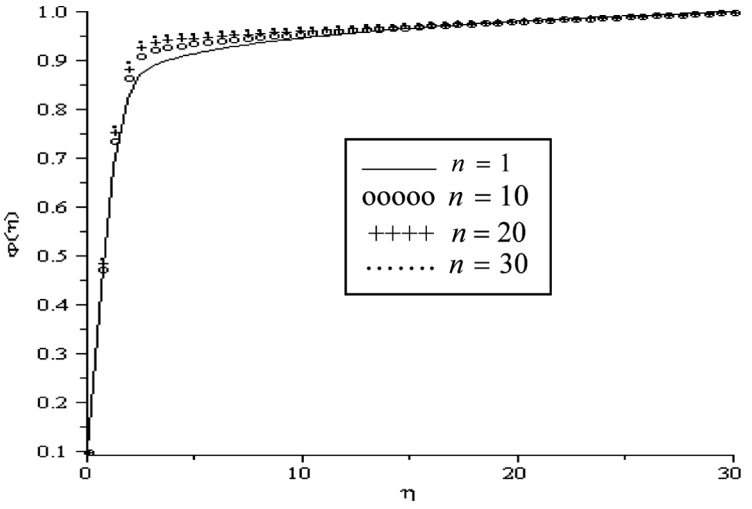

Figure 18. Effects of increasing reaction order on the concentration profiles when $Du = 0.3$, $Sr = 0.5$, $G_r = 1$, $G_c = 2$, $Ra = \gamma = Da = \theta_w = \varphi_w = c = 0.1$, $b = 1$, $Sc = 0.62$.

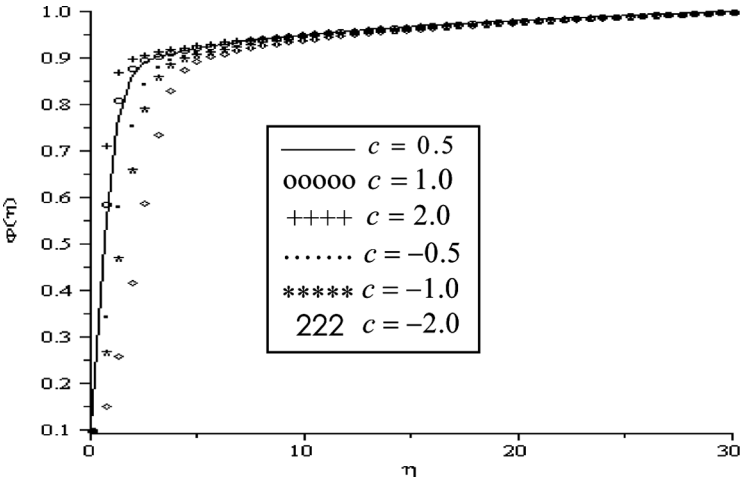

Figure 19. Variation of the boundary layer concentration profiles with increasing values of suction/injection parameter when $G_c = 2$, $G_r = 1$, $\gamma = Ra = Da = \theta_w = \varphi_w = 0.1$, $b = 1$, $n = 2$, $Du = 0.3$, $Sr = 0.5$, $Sc = 0.62$.

in parameter values of *Sr* and a decrease in the values of *Du* cause a decrease in the concentration of the chemical species in the boundary layer. Tsai and Huang (2009) reported similar observation on the effect of Sr and Du. Figure 17 is drawn for concentration profile versus η for different values of the Schmidt number *Sc*. We observed from this figure that the effect of Schmidt number *Sc* is to decrease the concentration distribution for lower values of *Sc* in the solutal boundary layer. As can be expected, the mass transfer rate decreases as *Sc* increases, with all other parameters fixed, that is, a decrease in the Schmidt number *Sc* decreases the concentration boundary layer thickness, which is associated with the reduction in the concentration profiles. Physically, the increase of *Sc* means a decrease of molecular diffusion *D*. Hence, the concentration of the species is higher for large values of *Sc* and lower for small values of *Sc*. A similar trend is observed with increasing value of reaction order index *n* (see Figure 18). It is interesting to note that an overshoot of concentration profile within the boundary layer occurs as *n* increases; this can be attributed to the fact that a significant decrease in the reacting species molecular diffusivity occurs due to higher order exothermic chemical kinetics within the concentration boundary layer. The effect of suction/injection parameter on the chemical species concentration in the boundary layer is depicted in Figure 19. From this figure, it is seen that the species concentration within the boundary layer is higher for suction and lower for injection.

Conclusions

In this work, we have studied numerically unsteady mixed convection with Dufour and Soret effects past a semi-infinite vertical porous flat plate moving through a binary mixture of chemically reacting fluid. Numerical solutions for the governing equations for momentum, energy, and concentration are given. Tabulated values and graphical representations are presented for the velocity, temperature, and

concentration profiles as well as local skin friction, local Nusselt number, and local Sherwood number. Our results reveal, among other points, that

- Local skin friction (C_f) increases with increasing parameter values of Ra, n, G_r, G_c, Sr, Du, Sc, $c > 0$ and decreases with increasing values of Sc, Da.
- Local Nusselt number (Nu) increases with increasing values of Da, Sr, $c > 0$ and decreases with increasing values of Sc, Ra, n, Du.
- Local Sherwood number increases with an increase in the values of Sc, Ra, n, Du, $c > 0$ and decreases with increasing values of Da, Sr.
- A reverse flow within the boundary layer is enhanced with an increase in the intensity of buoyancy forces, injection, destructive chemical reaction, radiation absorption, and thermo-diffusion (Soret) effect and a decrease in the diffusion-thermal (Dufour) effect.
- Fluid temperature increases while the species concentration decreases with an increase in Soret number and a decrease in Dufour number. Therefore, we can conclude that for fluids with medium molecular weight, like hydrogen-air mixtures, Dufour and Soret effects should not be neglected.

Acknowledgments

ODM would like to thank the National Research Foundation of South Africa Thuthuka program for financial support and the anonymous reviewers for their useful suggestions.

Nomenclature

b	heat generation parameter
C	concentration of the fluid
C_f	local skin friction parameter
C_w	surface concentration
C_∞	free stream concentration
c	suction parameter
c_p	specific heat at constant pressure
c_s	concentration susceptibility
D	diffusion coefficient; mass diffusivity
Da	Dämkohler number
Du	Dufour number
E	activation energy
G_c	local solutal Grashof number
G_r	local thermal Grashof number
g	gravitational acceleration
k	thermal conductivity
k_T	thermal diffusion ratio
Nu	local Nusselt number
Pr	Prandtl number
Q	heat generation coefficient
R_A	nth-order irreversible reaction
Ra	radiation parameter
R_G	universal gas constant

Sc Schmidt number
Sh local Sherwood number
Sr Soret number
T fluid temperature
T_m mean fluid temperature
T_w surface temperature
T_∞ free stream temperature
U_0 plate uniform velocity
(u, v) velocity components
(x, y) Cartesian coordinates

Greek Letters

α absorption coefficient
β thermal volumetric-expansion coefficient
β_c concentration volumetric-expansion coefficient
γ activation energy parameter
η similarity variable
θ fluid temperature
ρ fluid density
σ Stefan-Boltzmann constant
υ kinematic viscosity
φ fluid concentration

References

Abdallah, I. A. (2009). Analytic solution of heat and mass transfer over a permeable stretching plate affected by chemical reaction. Internal heating, Dufour-Soret effect and Hall effect, *Therm. Sci.*, **13**(2), 183–197.

Afify, A. A. (2009). Similarity solution in MHD: Effects of thermal diffusion and diffusion thermo on free convective heat and mass transfer over a stretching surface considering suction or injection, *Commun. Nonlinear. Sci. Numer. Simul.*, **14**, 2202–2214.

Alam, M. S., and Rahman, M. M. (2006). Dufour and Soret effects on mixed convection flow past a vertical porous flat plate with variable suction, *Nonlinear Anal. Model. Control*, **11**, 3–12.

Alam, M. S., Ferdows, M. S., Ota, M., and Maleque, M. A. (2006). Dufour and Soret effects on steady free convection and mass transfer flow past a semi-infinite vertical porous plate in a porous medium, *Int. J. Appl. Mech. Eng.*, **11**(3), 535–545.

Alam, M. S., Rahman, M. M., Ferdows, M., Kaino, K., Mureithi, E., and Postelnicu, A. (2007). Diffusion-thermo and thermal-diffusion effects on free convective heat and mass transfer flow in a porous medium with time dependent temperature and concentration, *Int. J. Appl. Eng. Res.*, **2**(1), 81–96.

Anghel, M., Takhar, H. S., and Pop, I. (2000). Dufour and Soret effects on free convection boundary-layer over a vertical surface embedded in a porous medium, *Stud. Univ. Babes-Bolyai Math.*, **45**(4), 11–21.

Bég, O. A., Bakier, A. Y., and Prasad, V. R. (2009). Numerical study of free convection magnetohydrodynamic heat and mass transfer from a stretching surface to a saturated porous medium with Soret and Dufour effects, *Comput. Mater. Sci.*, **46**, 57–65.

Chamkha, A. J., and Ben-Nakhi, A. (2008). MHD mixed convection-radiation interaction along a permeable surface immersed in a porous medium in the presence of Soret and Dufour's effect, *Heat Mass Transfer*, **44**, 845–856.

Chamkha, A. J., and Khaled, A. A.-R. (2000). Hydromagnetic combined heat and mass transfer by natural convection from a permeable surface embedded in a fluid saturated porous medium, *Int. J. Numer. Methods Heat Fluid Flow*, **10**(5), 455–476.

Chandrasekhara, B. C., Radha, N., and Kumari, M. (1992). The effect of surface mass transfer on buoyancy induced flow in a variable porosity medium adjacent to a vertical heated plate, *Heat Mass Transfer*, **27**(3), 157–166.

Chapman, S., and Cowling, T. G. (1952). *The Mathematical Theory of Non-uniform Gases*, 2nd ed., Cambridge Univ. Press, Cambridge.

Cheng, P. (1964). Two dimensional radiating gas flow by a moment method, *AIAA J.*, **2**(9), 1662–1664.

El-Aziz, M. A. (2008). Thermal-diffusion and diffusion-thermo effects on combined heat and mass transfer by hydromagnetic three-dimensional free convection over a permeable stretching surface with radiation, *Phys. Lett. A*, **372**(3), 263–272.

Ferdows, M., Kaino, K., and Crepeau, J. C. (2008). MHD free convection and mass transfer flow in a porous media with simultaneous rotating fluid, *Int. J. Dyn. Fluids*, **4**(1), 69–82.

Hirshfelder, J. O., Curtis, C. F., and Bird, R. B. (1954). *Molecular Theory of Gases and Liquids*, 1249, John Wiley, New York.

Jaluria, Y. (1980). *Natural Convection Heat and Mass Transfer*, 326, Pergamon Press, Oxford.

Schlichting, H. (1979). *Boundary Layer Theory*, 6th ed., 817, McGraw-Hill, New York.

Kafoussias, N. G., and Williams, E. W. (1995). Thermal-diffusion and diffusion-thermo effects on mixed free-forced convective and mass transfer boundary layer flow with temperature dependent viscosity, *Int. J. Eng.*, **33**, 1369–1384.

Kamenetskii, D. A. F. (1969). *Diffusion and Heat Transfer in Chemical Kinetics*, Plenum Press, New York.

Makinde, O. D. (2005). Free convection flow with thermal radiation and mass transfer past a moving vertical porous plate, *Int. Commun. Heat Mass Transfer*, **32**, 1411–1419.

Makinde, O. D., and Ogulu, A. (2008). The effect of thermal radiation on the heat and mass transfer flow of a variable viscosity fluid past a vertical porous plate permeated by a transverse magnetic field, *Chem. Eng. Commun.*, **195**(12), 1575–1584.

Ogulu, A., and Makinde, O. D. (2009). Unsteady hydromagnetic free convection flow of a dissipative and radiating fluid past a vertical plate with constant heat flux, *Chem. Eng. Commun.*, **196**(4), 454–462.

Postelnicu, A. (2007). Influence of chemical reaction on heat and mass transfer by natural convection from vertical surfaces in porous media considering Soret and Dufour effects, *Heat Mass Transfer*, **43**, 595–602.

Seddeek, M. A. (2004). Thermal diffusion and diffusion thermo effects on mixed free forced convective flow and mass transfer over an accelerating surface with a heat source in the presence of suction and blowing in the case of variable viscosity, *Acta Mech.*, **172**(1–2), 83–94.

Tsai, R., and Huang, J. S. (2009). Heat and mass transfer for Soret and Dufour's effects on Hiemenz flow through porous medium onto a stretching surface, *Int. J. Heat Mass Transfer*, **52**, 2399–2406.